Copyright © 2024 by the International Astronautical Federation (IAF). All rights reserved.

IAC–24–A3,IP,12,x85630

A Survey of Gravitational Modeling Techniques for Minor Body Proximity Operations

Carmine Buonagura[a*], Antonio Rizza[b], Carmine Giordano[c], Francesco Topputo[d]

[a] *PhD Student, Department of Aeropace Science and Technology (DAER), Politencico di Milano, Via La Masa 34, carmine.buonagura@polimi.it*
[b] *PhD Candidate, Department of Aerospace Science and Technology (DAER), Politencico di Milano, Via La Masa 34, antonio.rizza@polimi.it*
[c] *PostDoc Fellow, Department of Aerospace Science and Technology (DAER), Politencico di Milano,Via La Masa 34, carmine.giordano@polimi.it*
[d] *Full Professor, Department of Aerospace Science and Technology (DAER), Politencico di Milano, Via La Masa 34, francesco.topputo@polimi.it*
[*] *Corresponding author*

Abstract

The environment around a minor body is highly uncertain, depending on the body composition and shape, which are difficult to estimate from ground-based measurements. This paper addresses the challenges of operating in low-gravity, deep-space environments, focusing on gravitational modeling of minor bodies. The study reviews three primary modeling methods: spherical harmonics, the mascon model, and the polyhedral model, each with unique strengths and computational demands. These methods are tested on four well-known bodies: (101955) Bennu, (25143) Itokawa, (433) Eros, and 67P/Churyumov–Gerasimenko. The study evaluates the efficacy of each method in modeling gravitational forces, considering factors such as morphological uncertainties, shape knowledge, and computational complexity. The goal is to assist mission designers in selecting the most suitable model based on target properties and operational needs, thereby ensuring effective mission planning and execution in minor body exploration.

1. Introduction

Exploration of minor celestial bodies is increasingly attracting interest, prompting various space missions to target these objects due to the potential for significant scientific and engineering breakthroughs they offer [1–3]. Within this context, it becomes imperative to tackle the challenges inherent in operating in low-gravity, deep-space environments. A comprehensive understanding of the dynamics in the close proximity of these celestial objects becomes crucial for optimizing the scientific and technological yield of such missions. This is particularly relevant when employing cost-effective platforms like CubeSats, which operate with limited onboard resources and maneuvering capabilities. Therefore, thorough design and careful mission planning play a key role in maximizing the effectiveness of these missions. Particularly, accurate modeling and understanding of the gravitational field of minor bodies is crucial for space missions.

The environment in the vicinity of minor celestial bodies is characterized by significant uncertainties, arising from their irregular shapes, diverse morphologies, non-uniform mass distributions, and inaccurate estimations from ground-based observations [4, 5].

The shapes of small bodies can range from nearly spherical to ellipsoidal, elongated, or highly irregular. Furthermore, asteroids can span a variety of sizes and surface morphologies. Rubble-pile asteroids [6] are typically diamond-shaped and formed by the mutual gravity forces between various fragments, resulting in a substantial number of voids within the body volume. These asteroids are characterized by a high number of boulders scattered across their surface. Contact binary asteroids result from the collision of two bodies and may exhibit a notable density difference between the two components. Another category is the monolithic one, which consist of single rock fragments spinning rapidly. These are generally denser than rubble-piles and have fewer boulders on their surfaces. Comets, on the other hand, are usually characterized by a bilobed shape due to the presence of a melting ice nucleus. Their typical morphology consists of alternating smooth and rocky regions.

Moreover, there are significant uncertainties regarding the physical properties, overall shape, and morphology of small bodies because these are estimated from ground-based measurements, such as light-curve analysis and radar observations, when possible [7]. However, these measurements are often not accurate and provide only a preliminary idea of the body's shape, morphology, and composition [8]. As a result of the combination of these factors, the gravity model in the vicinity of these bodies is highly uncertain.

This paper explores three main modeling methods:

Copyright © 2024 by the International Astronautical Federation (IAF). All rights reserved.

spherical harmonics [9], mascon model [10–13], and polyhedral model [14]. The spherical harmonics method employs mathematical functions to represent the gravity of a body. The mascon model approximates the body mass distribution using discrete regions, simplifying computations. The polyhedral model, on the other hand, represent the body as a collection of polygons. Although each method offers unique advantages, researchers aim at simplifying the computational requirements for on-board implementation by conceptualizing different variants of these baseline methods.

This study conducts a comprehensive survey of various modeling techniques in the vicinity of four well-known minor bodies with diverse shapes, sizes, and masses, specifically (101955) Bennu, (25143) Itokawa, (433) Eros, and 67P/Churyumov–Gerasimenko. The research aims to support mission designers in selecting the most suitable approach based on the specific target properties and operative scenarios. Through extensive analysis, the study assesses the efficacy of each method in accurately modeling gravitational forces both inside and outside the Brillouin sphere of these minor bodies, defined as the sphere inscribing the object. It examines factors such as morphological uncertainties, shape knowledge, and the effects of body shape. Additionally, the study carefully considers computational complexity, accuracy, and suitability for on-board implementation. Understanding the strengths and limitations of each method is essential for successful planning of minor body exploration missions, whether prioritizing computational efficiency or accuracy.

The paper is structured as follows: Section 2 describes the general formulation of the gravity field with different estimation models. Section 3 outlines the methodology employed to compute the accuracy of each model. In Section 4, the accuracy and computational complexity of each model are assessed. Finally, Section 5 presents a discussion of some final considerations.

2. Gravity field models

In this section, the mathematical formulation of each of the analyzed models and some sub-models is discussed. The polyhedral model with 20,000 faces of the small bodies is considered as the true model for gravity field estimation. Specifically, the model is partitioned into a collection of simple tetrahedra, each with one vertex at the geometric center of the body and the opposite face represented by a triangular facet.

2.1 Polyhedral model

Regarding the polyhedral model, first introduced in [14], it uses the faces and edges of the polyhedral shape to compute the gravity field generated by the small body. The gravitational acceleration of this model can be computed as

$$\mathbf{a}_{\text{PM}} = -G\rho \sum_{e \in \text{edges}} \mathbf{E}_e \cdot \mathbf{r}_{\text{PM},e} L_e + G\rho \sum_{f \in \text{faces}} \mathbf{F}_f \cdot \mathbf{r}_{\text{PM},f} \omega_f \tag{1}$$

where G is the universal gravitational constant, ρ is the density of the body, $\mathbf{r}_{\text{PM},e}$ is a vector from the field point FP to a fixed point on edge e, $\mathbf{r}_{\text{PM},f}$ is a vector that extends from the field point to any point in the face plane f, and the dimensionless factor ω_f, for triangular faces, is defined as

$$\omega_f = 2\text{arctan}\left(\frac{\mathbf{r}_i \cdot \mathbf{r}_j \times \mathbf{r}_k}{r_i r_j r_k + r_i(\mathbf{r}_j \cdot \mathbf{r}_k) + r_k(\mathbf{r}_j \cdot \mathbf{r}_i)} \right) \tag{2}$$

where given a triangular face of the mesh of vertices P_i, P_j, and P_k, the vectors from the mesh geometric center and the vertices of the f face are $\mathbf{r}_i$, $\mathbf{r}_j$, and $\mathbf{r}_k$.
The dyads $\mathbf{E}_e$ and $\mathbf{F}_f$, and the scalar L_e are solely functions of the polyhedral model considered. $\mathbf{F}_f$ can be computed for each face of the polyhedron as

$$\mathbf{F}_f = \hat{\mathbf{n}}_f \circ \hat{\mathbf{n}}_f \tag{3}$$

where $\hat{\mathbf{n}}_f$ is the normal versor of the generic face f and $\circ$ represent the dyadic product, while $\mathbf{E}_e$ is computed for each edge and is defined as

$$\mathbf{E}_e = \hat{\mathbf{n}}_{f_1} \circ \hat{\mathbf{n}}_e^{f_1} + \hat{\mathbf{n}}_{f_2} \circ \hat{\mathbf{n}}_e^{f_2} \tag{4}$$

where $\hat{\mathbf{n}}_e^{f_1}$ and $\hat{\mathbf{n}}_e^{f_2}$ are the normals of the faces sharing the edge e, while $\hat{\mathbf{n}}_{f_1}$ and $\hat{\mathbf{n}}_{f_2}$ are the edge-normal vectors associated with the generic edge e. Finally, the dimensionless per-edge factor L_e is computed as

$$L_e = \ln \frac{r_i + r_j + e_{ij}}{r_i + r_j - e_{ij}} \tag{5}$$

where e_{ij} is the constant length of the edge connecting the points P_i and P_j.

An alternative version of the classic polyhedral model is presented in [15], where the mesh of the body is refined based on the position of the FP reducing the computational complexity of the model without a significant reduction in accuracy.

2.2 Mascon model

The mascon model is by far the most intuitive gravity computation as it considers the body gravity generated by multiple point mass. The position of the point masses is defined as the geometric center of each tetrahedron composing the shape model. The mass of each point is defined starting from the volume of each of them. By analytical calculation, the volume of the tetrahedron is given by the sixth part of the scalar triple product of the vectors repre-

Copyright © 2024 by the International Astronautical Federation (IAF). All rights reserved.

sented by three concurrent edges of this solid

$$V = \frac{1}{6}(\mathbf{r}_i \times \mathbf{r}_j \cdot \mathbf{r}_k) \tag{6}$$

Consequently, the mass and the associated gravitational constant μ for each tetrahedron can be computed through the knowledge of the density, usually assumed constant across the body volume. The gravitational acceleration suffered by the external point FP in relation to the model is

$$\mathbf{a}_{\text{MM}} = \sum_{i=1}^{n} -\frac{\mu_i}{r_{\text{MM},i}^3}\mathbf{r}_{\text{MM},i} \tag{7}$$

where $r_{\text{MM},i}$ is the distance between the centre of mass of the tetrahedron and the external point FP. The mascon model, differently from the other models can consider a variable density across the volume of the model.

Alternative versions divide the single tetrahedrons into M parts in order to obtain M layers with equal volume within each tetrahedron. The centroid of each figure is determined, and the mass is proportional to the volume of each figure. This approach increases the computational burden of the algorithm but increases its accuracy.

2.3 Spherical harmonics model

To compute the acceleration using the spherical harmonics model in the asteroid fixed frame, the gradient of the gravitational potential $U(\mathbf{x})$ must be determined.

$$\mathbf{a}_{\text{SH}} = \nabla U \tag{8}$$

Consequently, the potential U must be computed. Specifically, it can be represented as an infinite series of spherical harmonics, represented in a function space defined by the associated Legendre polynomials [16].

$$U = \frac{\mu}{r_{\text{SH}}}\sum_{n=0}^{\infty}\sum_{m=0}^{n}\left(\frac{R_0}{r_{\text{SH}}}\right)^n \overline{P}_{n,m}(u)\left(\overline{C}_{n,m}\cos(m\lambda) + \overline{S}_{n,m}\sin(m\lambda)\right) \tag{9}$$

with r, λ, and ϕ denote the radial distance from the minor body, the longitude, and the latitude of the spacecraft, respectively. The function $\overline{P}_{n,m}(u)$, where $u = \sin(\phi)$, represents the normalized associated Legendre polynomials [16]. R_0 serves as a scaling factor for computing the normalized coefficients $\overline{C}_{n,m}$ and $\overline{S}_{n,m}$.
The gradient of the potential can be expressed as [16]

$$\mathbf{a}_{\text{SH}} = \nabla U = \left[\frac{\partial U}{\partial \mathbf{r}_{\text{SH}}}\right]^T =$$

$$= \frac{\partial U}{\partial r_{\text{SH}}}\left[\frac{\partial r_{\text{SH}}}{\partial \mathbf{r}_{\text{SH}}}\right]^T + \frac{\partial U}{\partial \lambda}\left[\frac{\partial \lambda}{\partial \mathbf{r}_{\text{SH}}}\right]^T + \frac{\partial U}{\partial \phi}\left[\frac{\partial \phi}{\partial \mathbf{r}_{\text{SH}}}\right]^T =$$

$$= \left[\left(\frac{1}{r_{\text{SH}}}\frac{\partial U}{\partial r_{\text{SH}}} - \frac{z}{r_{\text{SH}}^2\eta}\frac{\partial U}{\partial \phi}\right)x - \left(\frac{1}{\eta^2}\frac{\partial U}{\partial \lambda}\right)y\right]\mathbf{i} +$$

$$+ \left[\left(\frac{1}{r_{\text{SH}}}\frac{\partial U}{\partial r_{\text{SH}}} - \frac{z}{r^2\eta}\frac{\partial U}{\partial \phi}\right)y + \left(\frac{1}{\eta^2}\frac{\partial U}{\partial \lambda}\right)x\right]\mathbf{j} +$$

$$+ \left[\frac{1}{r_{\text{SH}}}\frac{\partial U}{\partial r_{\text{SH}}}z + \frac{\eta}{r_{\text{SH}}^2}\frac{\partial U}{\partial \phi}\right]\mathbf{k} \tag{10}$$

where $\mathbf{r}_{\text{SH}} = x\mathbf{i} + y\mathbf{j} + z\mathbf{k}$ represents the field point location in minor body fixed frame, and $\eta = \sqrt{x^2 + y^2}$. The analytical expressions for $\frac{\partial U}{\partial r_{\text{SH}}}$, $\frac{\partial U}{\partial \lambda}$ and $\frac{\partial U}{\partial \phi}$ can be computed as [16, 17]:

$$\frac{\partial U}{\partial r_{\text{SH}}} = -\frac{\mu}{r_{\text{SH}}^2}\sum_{n=0}^{\infty}\sum_{m=0}^{n}\left(\frac{R_0}{r_{\text{SH}}}\right)^n (n+1)\,\overline{P}_{n,m}(u)\left(\overline{C}_{n,m}\cos(m\lambda) + \overline{S}_{n,m}\sin(m\lambda)\right) \tag{11}$$

$$\frac{\partial U}{\partial \lambda} = \frac{\mu}{r_{\text{SH}}}\sum_{n=0}^{\infty}\sum_{m=0}^{n}\left(\frac{R_0}{r_{\text{SH}}}\right)^n (n+1)\,\overline{P}_{n,m}(u)\,m\left(-\overline{C}_{n,m}\sin(m\lambda) + \overline{S}_{n,m}\cos(m\lambda)\right) \tag{12}$$

$$\frac{\partial U}{\partial \phi} = \frac{\mu}{r_{\text{SH}}}\sum_{n=0}^{\infty}\sum_{m=0}^{n}\left(\frac{R_0}{r_{\text{SH}}}\right)^n \frac{\partial \overline{P}_{n,m}(\sin(\phi))}{\partial \phi}\left(\overline{C}_{n,m}\cos(m\lambda) + \overline{S}_{n,m}\sin(m\lambda)\right) \tag{13}$$

$$\frac{\partial \overline{P}_{n,m}(\sin(\phi))}{\partial \phi} = \left[\frac{\partial \overline{P}_{n,m}(u)}{\partial u}\right]\cos\phi = \\ = -m\tan\phi\,\overline{P}_{n,m}(u) + K(n,m)\,\overline{P}_{n,m+1}(u) \tag{14}$$

and

$$K_{n,m} = \begin{cases} \sqrt{(n-m)(n+m+1)} & m > 0 \\ \sqrt{\dfrac{n(n+1)}{2}} & m = 0 \end{cases} \tag{15}$$

The coefficients $\overline{C}_{n,m}$ and $\overline{S}_{n,m}$ depend on the body

Copyright © 2024 by the International Astronautical Federation (IAF). All rights reserved.

shape and internal density distribution. In this study, they are assumed to be known for a given shape model and and are computed using the algorithm presented in [18]. The degree of expansion considered in this work is set to 16, implying a high level of knowledge about the body shape.

3. Methodology

The bodies selected for analysis span a variety of shapes, sizes, and morphologies: the nearly regular and rubble-pile asteroid (101955) Bennu, the bilobed and elongated (25143) Itokawa, the massive and irregular (433) Eros, and the highly irregular 67P/Churyumov–Gerasimenko, whose properties are reported in Table 1. For each body, a polyhedral model with 20,000 faces is

Table 1. Relevant properties of the minor bodies considered in this work.

Name	R_{eq} [km]	μ [km^3/s^2]	ρ [g/cm^3]
Itokawa	0.330	2.10×10^{-9}	1.900
67P	2.591	6.65×10^{-7}	0.533
Eros	17.62	4.46×10^{-4}	2.670
Bennu	0.282	4.67×10^{-9}	1.194

considered, and the polyhedral gravity model of this high-resolution model is assumed to be the true gravity of the body. This means that all errors and accuracies of the other models are computed relative to this baseline scenario. As previously discussed, high-resolution models are not always available, particularly from ground-based measurements. To account for uncertainties in the available shapes, models with 2,000 faces are used in this work.

To assess the performance of each model, a zero-finding problem is solved to determine 16 iso-gravity surfaces surrounding the minor body. These surfaces are regions in space where the gravity field induced by the body is constant. Specifically, for each analyzed body, 10 iso-gravity surfaces were computed inside the Brillouin sphere, while 6 were computed outside of it. To find these surfaces, each normal of the mesh vertices is multiplied by a value ξ_i, which ranges from 0 to an arbitrarily high value, to determine the displacement needed to achieve a gravity equal to a prescribed value a_0.

$$f(\xi_i) = a_b(\xi_i) - a_0 \tag{16}$$

where a_b is the gravity induced by the 20,000-face mesh model. The locus of the obtained points forms an iso-surface that is likely to have an irregular shape. The furthest iso-gravity surface is defined as the one where the gravity is computed at 10 equivalent radii from the body center of mass, assuming that at this distance the gravity induced by the body shape is negligible and the point mass gravity approximation is valid. Four iso-gravity surfaces inside the Brillouin sphere of asteroid (25143) Itokawa are shown in Figure 1.

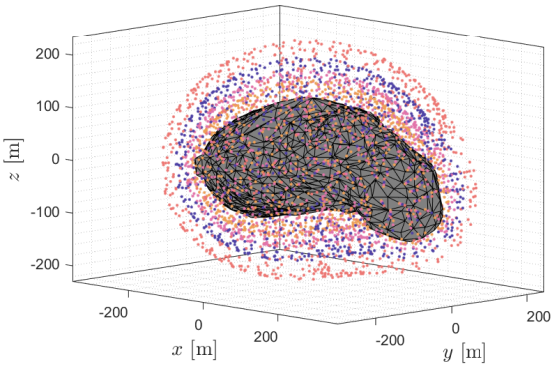

Fig. 1. Example of four iso-gravity surfaces inside the Brillouin sphere of asteroid (25143) Itokawa.

Different scenarios are considered, to take into account morphology uncertainties and the influence of the shape on the gravity estimation

Firstly, morphology uncertainties are taken into account by perturbing the mesh of 2,000-face available shape model randomly displaying the vertices of the original model $\mathbf{v}_0$ along their normals $\mathbf{n}_0$

$$\hat{\mathbf{v}}_i = \mathbf{v}_{0,i} + \sigma_u \mathbf{n}_{0,i} \tag{17}$$

where $\hat{\mathbf{v}}_i$ represents the final vertex position of the ith vertex and σ_u is a zero-mean white Gaussian noise with variance Q.

$$\sigma_u = \mathcal{N}(0, Q) \tag{18}$$

where the variance Q is a value depending on the minor body equivalent radius R_{eq}:

$$Q = 0.05 R_{eq} \tag{19}$$

Secondly, all three baseline models are tested on shape models with different resolutions: specifically, 2,000, 1,000, 500, and 100 faces. This helps assess the robustness of the models in the face of increasingly poor knowledge of the body shape model. The figure of merit for gravity estimation error considered in this analysis is the Root Mean Square Error (RMSE) with respect to the constant gravity a_0 for each iso-gravity surface. The error is defined as:

Copyright © 2024 by the International Astronautical Federation (IAF). All rights reserved.

$$\text{RMSE} = \sqrt{\frac{1}{N}\sum_{i=1}^{N}(a_{\text{M},i} - a_0)^2} \qquad \text{with} \quad \text{M} \in \{\text{PM}, \text{MM}, \text{SH}\} \tag{20}$$

where N represent the number of points belonging to an iso-gravity surface and $a_{\text{M},i}$ is the estimated gravity at the ith point, with model M.

It is worth noting that the mass of the models is kept constant, and the density is iteratively computed based on the volume of the given mesh.

4. Results

In this section, the results will be presented for the four minor bodies considered in this work.

The three gravity estimation models will be applied to the 2,000-face shape models, using Monte Carlo analysis to account for morphological uncertainties by perturbing their vertices.

Additionally, different resolutions of the minor body mesh will be analyzed to assess the performance of each method under progressively poorer shape knowledge.

The point mass gravity model will also be reported for each examined case. All models should converge to this point mass model as the distance from the small body increases, serving as an upper bound for gravity estimation error. This means that the error for all considered models must be below the corresponding point mass value to demonstrate an improvement in gravity estimation.

4.1 Morphology uncertainty

In this section, the polyhedral, mascon, and spherical harmonics models are tested on the four small bodies, with perturbations applied to their vertices to account for variations in surface morphology. The results of this analysis are presented in Figure 2.

When in close proximity to a minor body, within the Brillouin sphere, the spherical harmonics model struggles to accurately estimate gravity because the expansion fails to converge, resulting in larger estimation errors than those of the point mass model. (101955) Bennu is the only body for which it is possible to compute the gravity within the Brillouin sphere using spherical harmonics, due to its regular shape.

The polyhedral model provides the most accurate gravity estimation for most bodies, followed by the mascon model. However, (101955) Bennu is an exception, where the mascon model slightly outperforms the polyhedral model.

As expected, the spherical harmonics model performs poorly inside the Brillouin sphere but significantly improves at its boundary, surpassing the other models as the distance from the small body increases.

The analysis suggests that morphology uncertainties play a key role, particularly for (101955) Bennu and 67P/Churyumov–Gerasimenko, where covariance bounds appear more dispersed compared to (433) Eros and (25143) Itokawa, especially at lower gravity values farther from the minor body.

From a computational perspective, the spherical harmonics model is the most efficient, outperforming the polyhedral and mascon models by an order of magnitude, as shown in Table 2.

4.2 Shape uncertainty

In this section, different resolutions of the minor body meshes are considered to assess the performance of the models based on shape estimation. As expected, and shown in Figure 3, the performance of each model decreases as the number of faces in the model mesh is reduced. Notably, for (101955) Bennu and 67P/Churyumov–Gerasimenko, the estimation error with 100 faces exceeds that of the point mass model, indicating that accurate knowledge of the minor body's preliminary shape is crucial. This suggests the need for a preliminary shape model estimation phase before proximity operations.

From 500 faces onward, the model's performance improves, providing good estimations with only slightly higher error compared to the most refined model with 2,000 faces.

From a computational perspective, the spherical harmonics model is unaffected by the mesh resolution, consistently maintaining a lower computational burden. In contrast, the polyhedral and mascon models reduce computational effort as mesh resolution decreases. However, they only reach the computational speed of the spherical harmonics model when using low-resolution meshes, and never surpass it. The computational times* for each of the considered mesh resolutions are reported in Table 2.

Table 2. Computational time depending on the model resolution in terms of number of faces N_f and gravity model.

Times in seconds		**Models**		
		PM	MM	SH
Res $[N_f]$	2,000	7.3×10^{-4}	5.2×10^{-4}	2.7×10^{-5}
	1,000	3.6×10^{-4}	2.7×10^{-4}	2.3×10^{-5}
	500	1.8×10^{-4}	1.6×10^{-4}	2.4×10^{-5}
	100	3.3×10^{-5}	5.7×10^{-5}	2.1×10^{-5}

*Six-core Intel i7@2.20GHz

Copyright © 2024 by the International Astronautical Federation (IAF). All rights reserved.

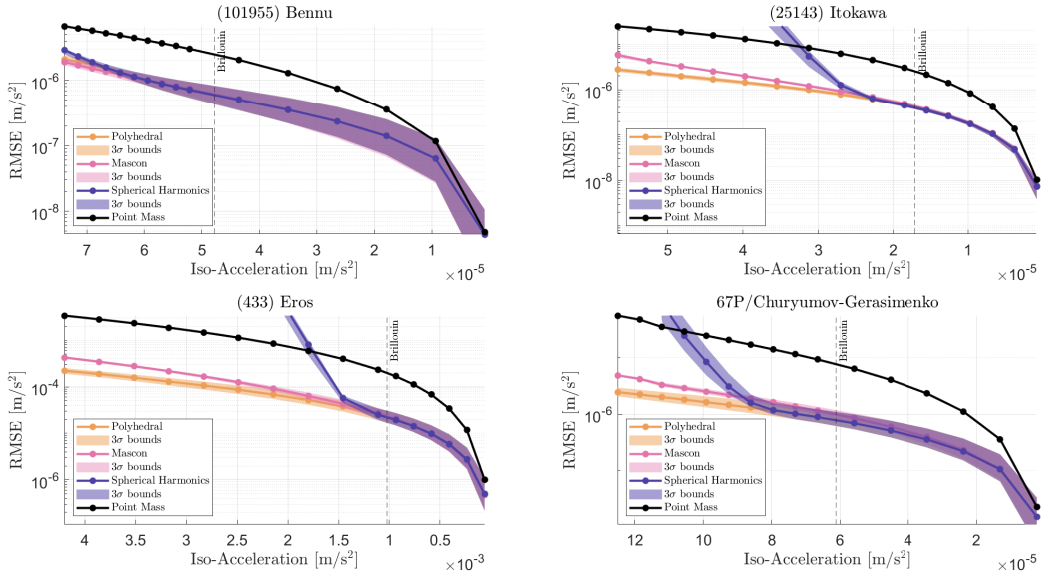

Fig. 2. Gravity models error with bodies of different morphologies.

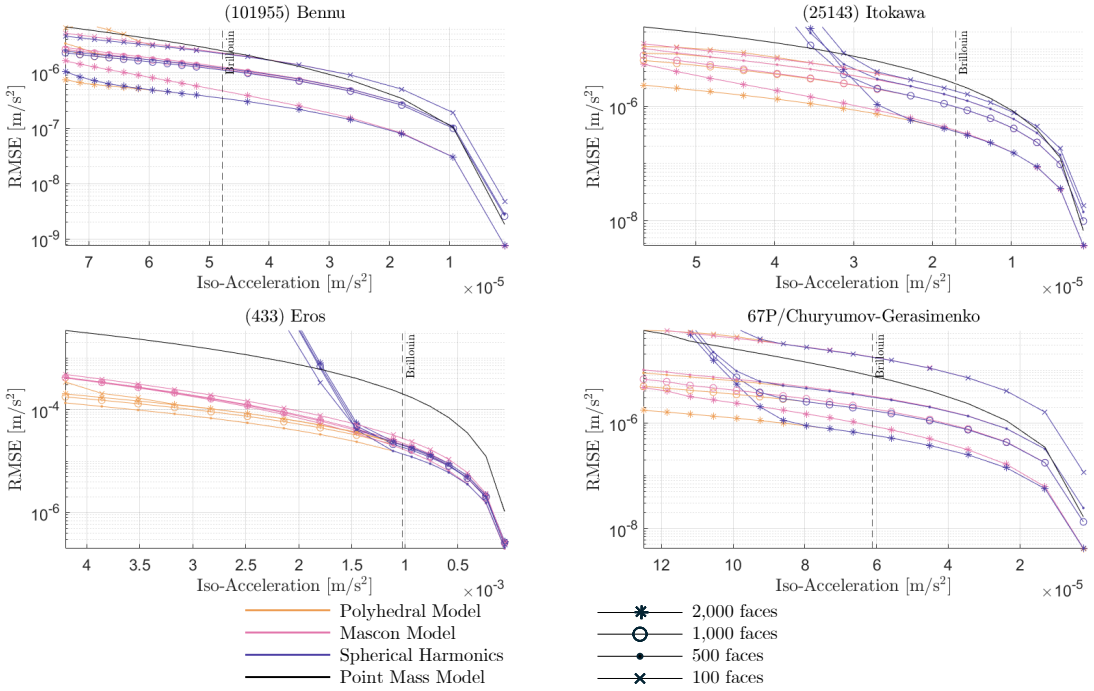

Fig. 3. Gravity models error with bodies of different resolutions.

5. Conclusions

This study highlights the importance of selecting appropriate gravitational models when exploring minor celestial bodies, which are gaining attention for their scientific and engineering potential. By comparing the spherical harmonics, mascon, and polyhedral models on bodies such as (101955) Bennu, (25143) Itokawa, (433) Eros, and 67P/Churyumov–Gerasimenko, the research underscores

Copyright © 2024 by the International Astronautical Federation (IAF). All rights reserved.

the strengths and limitations of each method. The polyhedral model excels in close proximity within the Brillouin sphere, while the spherical harmonics model offers comparable accuracy at a lower computational cost outside the sphere. The analysis also reveals that shape uncertainties significantly affect gravity field estimations. Accurate shape knowledge is essential, as poor models can lead to worse performance than the point mass model. Ultimately, the spherical harmonics model stands out for its computational efficiency, providing valuable insights for mission planners in low-gravity environments.

6. References

[1] M. Quadrelli *et al.*, "Guidance, navigation, and control technology assessment for future planetary science missions," *Journal of Guidance, Control, and Dynamics*, vol. 38, no. 7, pp. 1165–1186, 2015. DOI: https://doi.org/10.2514/1.G000525.

[2] E. Asphaug, "Growth and evolution of asteroids," *Annual Review of Earth and Planetary Sciences*, vol. 37, pp. 413–448, 2009. DOI: https://doi.org/10.1146/ANNUREV.EARTH.36.031207.124214.

[3] K. Zacny, P. Chu, J. Craft, M. Cohen, W. James, and B. Hilscher, "Asteroid mining," in *AIAA SPACE 2013 Conference and Exposition*, 2013.

[4] W. F. Bottke Jr, A. Cellino, P. Paolicchi, and R. P. Binzel, "An overview of the asteroids: The asteroids iii perspective," *Asteroids III*, vol. 1, pp. 3–15, 2002.

[5] D. J. Tholen and M. A. Barucci, "Asteroid taxonomy.," *Asteroids II*, pp. 298–315, 1989.

[6] K. J. Walsh, "Rubble pile asteroids," *Annual Review of Astronomy and Astrophysics*, vol. 56, no. 1, pp. 593–624, 2018. DOI: 10.1146/annurev-astro-081817-052013.

[7] D. Scheeres, *Orbital motion in strongly perturbed environments: applications to asteroid, comet and planetary satellite orbiters*. Springer Berlin, Heidelberg, 2016, Chapter 1-2. DOI: https://doi.org/10.1007/978-3-642-03256-1.

[8] C. Buonagura, C. Giordano, F. Ferrari, and F. Topputo, "The Orbital Regime Index: a Comprehensive Parameter to Determine Orbital Regions Around Minor Bodies," in *47th Rocky Mountain AAS GN&C Conference*, 2024.

[9] R. A. Werner, "Spherical harmonic coefficients for the potential of a constant-density polyhedron," *Computers & Geosciences*, vol. 23, no. 10, pp. 1071–1077, 1997, ISSN: 0098-3004. DOI: https://doi.org/10.1016/S0098-3004(97)00110-6.

[10] P. T. Wittick and R. P. Russell, "Mixed-model gravity representations for small celestial bodies using mascons and spherical harmonics," *Celestial Mechanics and Dynamical Astronomy*, vol. 131, pp. 1–29, 2019. DOI: https://doi.org/10.1007/s10569-019-9904-6.

[11] T. Chanut, S. Aljbaae, and V. Carruba, "Mascon gravitation model using a shaped polyhedral source," *Monthly Notices of the Royal Astronomical Society*, vol. 450, no. 4, pp. 3742–3749, 2015. DOI: https://doi.org/10.1093/mnras/stv845.

[12] M. Antoni, "A review of different mascon approaches for regional gravity field modelling since 1968," *History of Geo- and Space Sciences*, vol. 13, no. 2, pp. 205–217, 2022. DOI: https://doi.org/10.5194/hgss-13-205-2022.

[13] S. Tardivel, "The limits of the mascons approximation of the homogeneous polyhedron," in *AIAA/AAS Astrodynamics Specialist Conference*, 2016.

[14] R. A. Werner and D. J. Scheeres, "Exterior gravitation of a polyhedron derived and compared with harmonic and mascon gravitation representations of asteroid 4769 Castalia," *Celestial Mechanics and Dynamical Astronomy*, vol. 65, pp. 313–344, 1996. DOI: https://doi.org/10.1007/BF00053511.

[15] A. Pedros-Faura and J. W. McMahon, "Mixed fidelity shape models for efficient small body gravity modeling," *Journal of Guidance, Control, and Dynamics*, vol. 47, no. 2, pp. 247–261, 2024. DOI: https://doi.org/10.2514/1.G007617.

[16] D. A. Vallado, *Fundamentals of astrodynamics and applications*. Springer Science & Business Media, 2001, vol. 12, ISBN: 978-1-881883-14-2.

[17] J. B. Lundberg and B. E. Schutz, "Recursion formulas of legendre functions for use with nonsingular geopotential models," *Journal of Guidance, Control, and Dynamics*, vol. 11, no. 1, pp. 31–38, 1988. DOI: https://doi.org/10.2514/3.20266.

Copyright © 2024 by the International Astronautical Federation (IAF). All rights reserved.

[18] A. Rizza, C. Buonagura, P. Panicucci, and F. Topputo, "Modular Pipeline for Small Bodies Gravity Field Modeling: Enhancing accuracy and efficiency for proximity operations," in *75th International Astronautical Congress 2024 (IAC2024)*, 2024. DOI: https://doi.org/10.48550/arXiv.2409.02531.